

Analysis of Crushing Response of Composite Crashworthy Structures

Matthew David · Alastair F. Johnson · H. Voggenreiter

Received: 11 September 2012 / Accepted: 25 October 2012 / Published online: 28 November 2012
© Springer Science+Business Media Dordrecht 2012

Abstract The paper describes quasi-static and dynamic tests to characterise the energy absorption properties of polymer composite crash energy absorbing segment elements under axial loads. Detailed computer tomography scans of failed specimens are used to identify local compression crush failure mechanisms at the crush front. The varied crushing morphology between the compression strain rates identified in this paper is observed to be due to the differences in the response modes and mechanical properties of the strain dependent epoxy matrix. The importance of understanding the role of strain rate effects in composite crash energy absorbing structures is highlighted in this paper.

Keywords Composite structures · Crashworthiness · Energy absorption · Crush test method · Composites failure modes · Dynamic crushing response

1 Introduction

The increase usage of polymer composite materials in the aerospace and automotive industry has generated considerable interest in using composite materials for crashworthy structures that have the ability to absorb impact energy through a controlled failure in progressive crushing. By tailoring the fibre type, matrix type, fibre-matrix interface, fibre stacking sequence and fibre orientation, composite crashworthy structures have been shown to have excellent energy absorption performance characteristics [1, 2]. To understand the energy absorption and failure mechanisms of crashworthy structures, the German Aerospace Center (DLR) has developed a chamfered tube segment specimen [3], which is easy to fabricate and gives reproducible axial crush failures under quasi-static and dynamic loading conditions [4]. This may be used for screening of different energy absorbing composite materials and provides design data for crashworthy design studies. The paper describes a successful methodology for

M. David (✉) · A. F. Johnson · H. Voggenreiter
German Aerospace Center (DLR), Institute of Structures and Design,
Pfaffenwaldring, 38-40, Stuttgart, Germany
e-mail: matthew.david@dlr.de

crush testing of chamfered tube segment specimens in both quasi-static and dynamic loading conditions with an analysis method to compare the varied crushing characteristics and energy absorption performances between the two loading conditions. Tests on the chamfered tube segment specimens are presented in detail, with particular emphasis on the influence of loading rate on energy absorbed and crush failure mechanisms. The testing methodology includes the use of a high speed camera to capture the crushing behaviour of the specimen during the crush tests. In addition to capturing the crushing behaviour of the specimen, High-resolution Computed Tomography (HRCT) scanning of the specimen was performed to enable a detailed analysis of crushed specimen using the nanotom[®] CT system by phoenix xray. This permits detailed observation of the composites failure surface by X-ray without the need for sectioning and microscopic analysis.

From reviewing current literature, the lack of consensus about the influence of loading rate on the energy absorption performances of a composite material in varied material systems was identified [5–8]. Kindervater [9] suggested that the influence of the loading rate on the energy absorption performances is dependent on the material system. For carbon-epoxy tubes, a reduction in the energy absorption performance was recorded in dynamic crush tests up to 9.0 m/s. This behaviour was unlike the dynamic crush tests of high performance polyethylene-epoxy tubes, where a 50.0 % increase in the energy absorption performance was observed. Based on tests conducted on carbon-epoxy tubes by Farley [10], Mamalis et al. [11] suggested that for the $[0/\pm\theta]_2$ carbon-epoxy tubes, the strain-rate independent fibre properties control the crushing process and for the $[\pm\theta]_3$ carbon-epoxy tubes, the strain-rate dependent matrix properties control crushing. Jacob et al. [12] identified that at very high loading rates, the structure responds in a local mode and therefore the strain energy absorbing capabilities of the fibres is less important to the impact resistance of composites. This paper aims to study this local mode phenomenon in detail and its effect on composite crashworthy structures with a carbon-epoxy material system.

2 Test Specimens

The geometry of the test specimen was based on previous work by DLR [3]. Figure 1 presents a sketch of this geometry. The test specimen consists of three segments, half circle segment and two flanges (each comprising of a rectangular segment and a quarter circle segments). These specimens were manufactured from Hexply M18/1/43 %/G939/1230 five harness fabric prepreg material. The ply layup composed of nine plies with a $[(0/90)_2/0/(90/0)_2]$ configuration. A female tool was used to lay up the plies before the autoclave curing process. The trigger mechanism of these test specimens was a 45.0° outside chamfer, machined using a custom built tooling. This mechanism allows the crushing process to initiate in the highly stressed region at the tip of the chamfer and then develop into a stable crush zone.

3 Test Methodology

3.1 Quasi-static Crush Test

The quasi-static crush test was conducted on a Zwick Roell AG Static Test machine with a 100.0 kN load cell. Figure 2a and b shows the test setup together with the test specimen

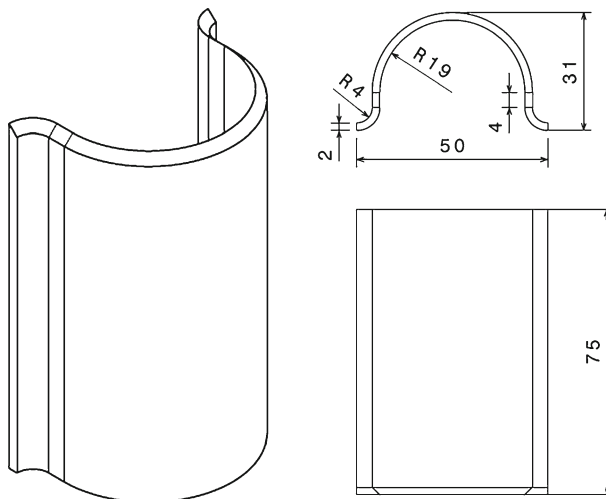


Fig. 1 Sketch of DLR segment test specimen

before and after the quasi-static crush test respectively. All the following crush tests (quasi-static and dynamic) presented here were conducted within the range of the recommended control conditions for the testing of composites.

The test specimen affixed in a clamp support was placed on a lower steel platen with the bevel edge end up as shown in Fig. 2a. This lower steel platen which remains stationary during the crush test was connected to the load cell. During the quasi-static crush test, the upper steel platen affixed to the crosshead, moves down to the test specimen and the crushing process is initiated; see Fig. 2b. The cross head velocity was 1 mm/s which correspond to a compression strain rate of 0.0133 s^{-1} . Upon the commencement of the crush test, the crush load, cross-head velocity, and cross-head displacement were recorded and output as ASCII files. Recording of these data was done at a frequency of 10.0 Hz. Each individual crush test was filmed with a Photron Fastcam Ultima APX 250K. Recording of the crushing processes was programmed at 9000 fps with a shutter speed of $1/9000 \text{ s}$. The test specimens were spray painted with a light coat of white to provide a good contrast with the background as the recording was done in mono. From analysing the crushing process, the test specimens exhibited a crushing behaviour consisting of three phases, crushing down

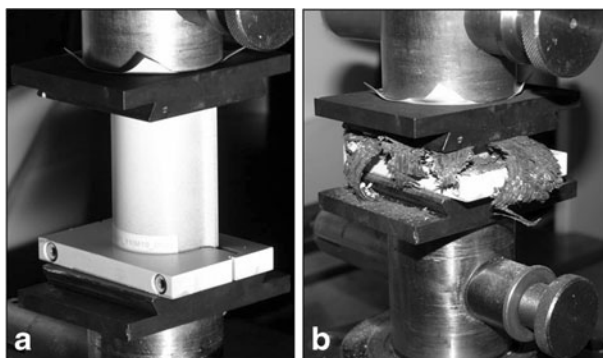


Fig. 2 Quasi-static crush test setup

of trigger portion, splaying of the lamina bundles and the axial splitting of the outer lamina bundle into fronds. Figure 3a to f presents the images extracted from the recording of the quasi-static crush test of the test specimen. Once the trigger portion is crushed down, *see* Fig. 3a, lamina bundles were seen to splay, *see* Fig. 3b into two distinct portions (inner and outer lamina bundles). The splaying causes the axial splitting to initiate in the outer lamina bundle as seen at the crush front in Fig. 3b. As the crushing process continues, the outer lamina bundle, due to the axial splitting, causes the outer lamina bundles to split into several petal-like portions called fronds. Figure 3c shows the start of these fronds and Fig. 3d to f presents the steady state crushing phase of the crushing process by means of the propagation of these fronds. The inner lamina bundle, splits into fronds similar to the behaviour of the outer lamina bundle but due to the geometry of the test specimen, these fronds collide into each other and were seen to curl up during the crushing process. These inner and outer fronds are clearly seen in Fig. 4 which shows this crushed test specimen.

3.2 Dynamic Crush Test

Dynamic crush tests were conducted on an Instron VHS 100/20 High Strain Rate Test machine with a 100.0 kN load cell. Figure 5a and b show respectively the test setup together with the segment specimen just before and after the impact for the dynamic crush test conducted with an impact velocity of 2.0 m/s.

The test specimen affixed in a clamp support was placed on a lower steel platen with the bevel edge end up, *see* Fig. 5a. This lower steel platen was connected to the cross-head which is displacement controlled during the dynamic crush test and moves the test specimen up to impact onto the stationary upper platen which was affixed to the load cell; *see* Fig. 5b. Impact velocity was specified using the test machine software, in which a displacement-time pulse is prescribed to reach the required impact velocity at the cross-head upon the contact of the upper steel platen with the test specimen. This velocity is held constant for most of the test before being reduced to zero at a specified stroke length. During the test, the crush load,

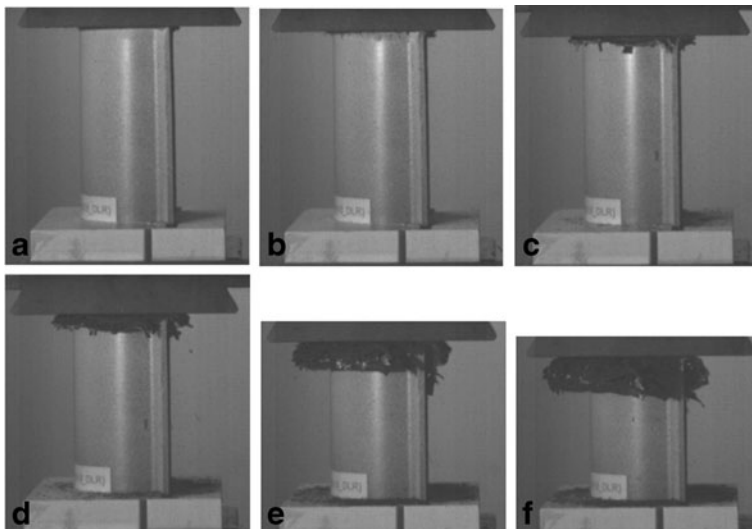
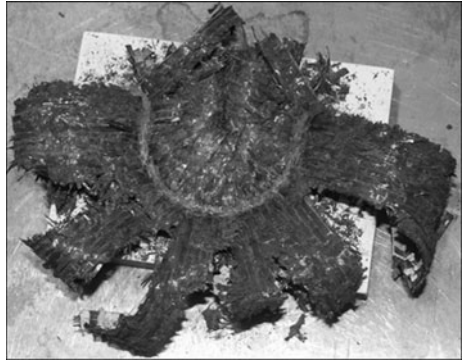


Fig. 3 Quasi-static crushing process

Fig. 4 Test specimen (I) after the quasi-static crush test



cross-head velocity, and cross-head displacement were recorded and output as ASCII files with a sampling frequency of 10 Hz. The compression strain rates for the dynamic crush tests conducted are as follows, 15.3 s^{-1} (impact velocity 2.0 m/s), 42.5 s^{-1} (impact velocity 5.0 m/s) and 74.4 s^{-1} (impact velocity 10.0 m/s). Crush test was filmed with the Photron Fastcam Ultima APX 250K as before. From analysing the crushing process of the three dynamic crush tests conducted, it was observed that the test specimens exhibited a similar crushing behaviour for the three test velocities. This comprised of three phases, crushing down of trigger portion, splaying of the lamina bundles and the fragmentation of these lamina bundles. Figure 6a to d presents the images of the dynamic crush test of specimen (IV) at an impact velocity of 10.0 m/s^{-1} . Figure 6a displays the test specimen just before impact. Upon impact with the load cell, a shock wave was observed to propagate from the crush front to the end of the test specimen. The period of the crushing process when the trigger portion is crushed down and the splaying (highlighted with a dotted circle) of the test specimen into two lamina bundles (inner and outer) at the crush front is shown in Fig. 6b. Figure 6c and d show the start of the steady state crushing phase (fragmentation of the lamina bundles) and the steady state crushing phase respectively. Figure 7 presents this test specimen (IV) after the dynamic crush test. The crushed test specimens in the other impact velocity cases also exhibit similar crush characteristics. Loose debris from the fragmentation process was collected in the inner portion of the test specimens and was observed to reduce with an increase in the impact velocity.

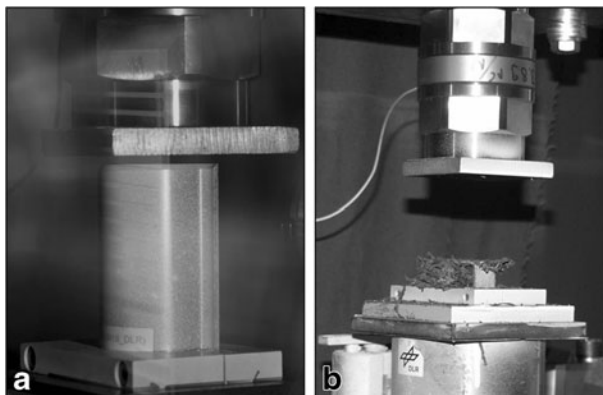


Fig. 5 Dynamic crush test setup

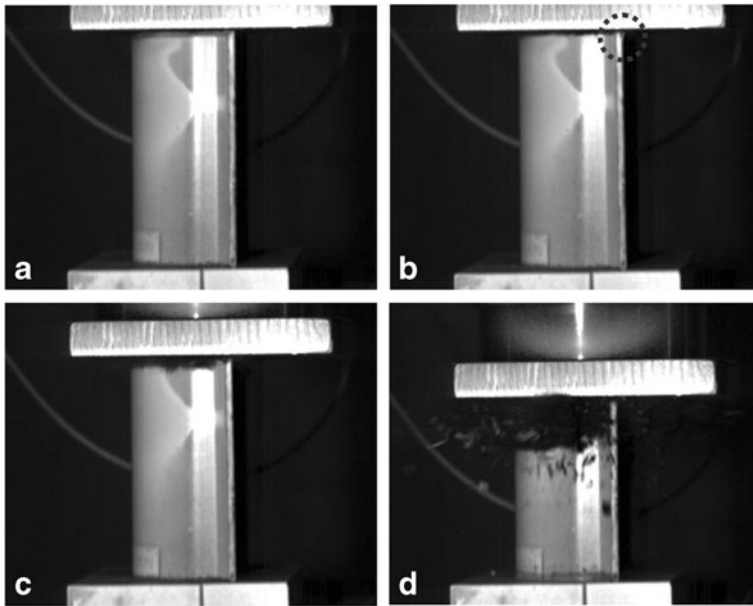
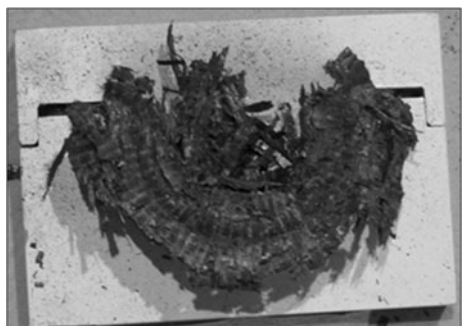


Fig. 6 Dynamic crushing process in specimen (IV) at an impact velocity of 10.0 m/s

3.3 HRTC Scanning of Test Specimens

To enable a detailed analysis of the varied crushed test specimens from the dynamic and quasi-static crush test, HRCT scanning of the test specimens (I and IV) were performed using the nanotom[®] CT system by phoenix xray. The voxel resolution used in the scanning of the test specimens was 7 μm . Generating the tomography images starts with the acquisition of two dimensional X-ray images. A collection of these images is acquired by rotating the test specimens in 1.0° steps through a full 360.0° . These projections contain information on the features within the test specimens. This accumulation of data is then used for the numerical reconstruction of the volumetric data. The reconstruction is performed parallel to the acquisition process. Resulting volume data set is then visualized by slices perpendicular to the three dimensions or compiled in a three-dimensional view which can be displayed in various ways. For each of the test specimens scanned, the total time from the acquisition phase to the reconstruction of the volumetric data took approximately 5.0 h. The

Fig. 7 Test specimen (IV) after the dynamic crush test



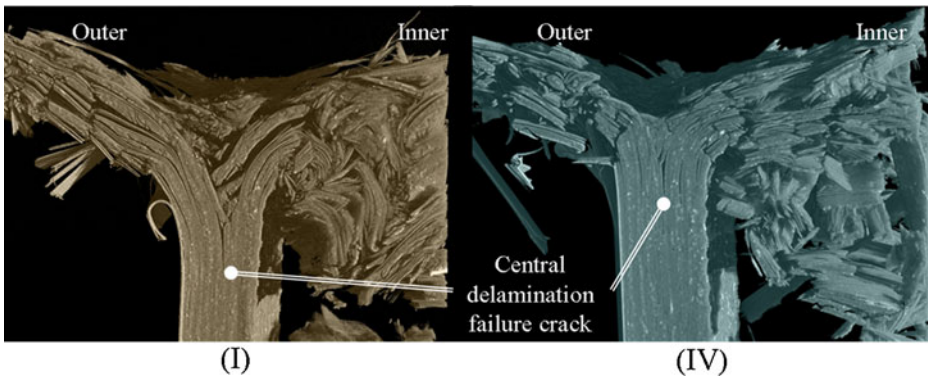


Fig. 8 HRCT-scan image of test specimen (I) quasi-static and (IV) dynamic

results of these HRCT scans are presented in Fig. 8 which corresponds to the test specimen (I) and the test specimen (IV).

4 Results and Discussion (a)

Crush force efficiency (CE), Energy Absorbed (EA) and Specific Energy Absorbed (SEA) were chosen to measure the energy absorption performance of the crush tubes in the quasi-static and dynamic tests. CE also known as the crush force ratio [13] is the ratio of the peak crush force to the steady state crush force SSCF. A crush force efficiency value close to 1 is desired as this would minimise the imparting of large forces on to the overall structure (i.e. helicopter sub-structure) during the crush initiation. EA represents the total area under the crush force-displacement curve for the entire crushing process, which was obtained by numerical integration of the curve. SEA is the energy absorbed per unit mass of the test specimen. This was calculated by dividing EA with the mass of the crushed portion of the test specimen.

Figure 9 presents the crush load–displacement curves of the crush tubes analyzed in this investigation. Table 1 summarizes the energy absorption performances of these test specimens for the entire duration of the crushing process. The steady state crushing phase is a region of interest in the field of crashworthiness as the energy absorbing structure (test specimen) is collapsing in a stable, progressive manner and its behavior controlled by energy absorbing mechanisms. As Fig. 9 clearly shows the SSCF is fairly constant for the three dynamic tests, with a value that is significantly lower than in the quasi-static test. In Table 1 it is shown that CE ranges from 1.33 for the quasi-static test up to 1.98 for the 10.0 m/s test. This is caused by the higher initial peak forces found in the dynamic tests together with a lower steady crush force compared with those in the quasi-static test. The SSCF obtained from the quasi-static test is the highest from all the crush tests conducted with 35.7 % increase in SSCF when compared between the impact velocity of 2.0 m/s and the quasi-static crush test. The EA obtained from the quasi-static test is the highest of all the crush tests (59.4 % increase when compared to the impact velocity of 2.0 m/s). This increase can be partially attributed to the larger crushing displacement, which depends on the assigned stroke length in the input pulse. The SEA calculated, would therefore take this large crushing displacement into account and it is shown that only a 28.3 % increase in SEA exists between the quasi-static crush test and the impact velocity of 2.0 m/s. Additionally, increasing the

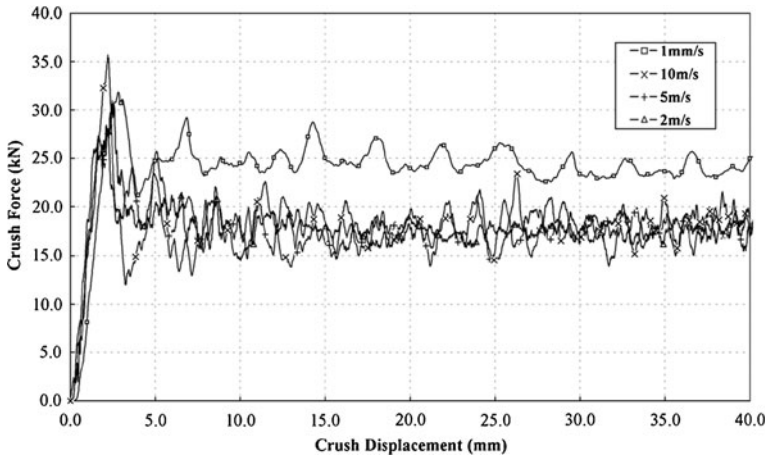


Fig. 9 Crush force versus Crush displacement

compression strain rates (15.3 s^{-1} to 74.4 s^{-1}) brought about a slight reduction in the SEA from 0.53 % (2.0 m/s to 5.0 m/s) to 1.25 % (2.0 m/s to 10.0 m/s).

The quasi-static and the dynamic crushing process had similar characteristics to the crushing process known as the splaying mode as described by Hull [14] which is characterized by very long interlaminar, intralaminar and parallel-to-fibre cracks with little or no fracture of the axial lamina bundles. During this crushing process, the trigger portion is crushed down at the crush front. An annular wedge of highly compacted and fragmented debris (debris wedge) is forced axially through the tube wall during the crushing down of the trigger portion. Once the trigger portion is fully crushed down, the splaying of the lamina bundles into two distinct portions (inner and outer lamina bundles) is initiated by this debris wedge below which a central crack propagates. In the quasi-static crushing process, the splayed lamina bundles exhibit axial splitting and form petal like portions called fronds due to the formation of equally spaced axial cracks along the circumference of the composite tube. These axial cracks are due to the expansion of the outer lamina bundles which increases the hoop stress and therefore involves the fibre fracture of the transverse fibres and the tensile fracture of the axial fibres as described by Hull. In the dynamic crushing process however, the splayed lamina bundles fracture at the base of the lamina bundles with no axial splitting and therefore large amount of fragmentation of the test specimen was observed during the dynamic crush test compared with the quasi-static test.

4.1 Response Mode

From analyzing the HRCT-scan image of the test specimen in the dynamic crush test Fig. 8, the damage of the test specimens in the form of interlaminar and intralaminar delaminations was located close the crush front (local) and formed by the bending of plies, without a significant fibre debris wedge. This is unlike in the HRCT-scan image of the test specimen in the quasi-static crush test (see Fig. 8) where the extent of the damage extended further away from the crush front (global) where, the debris wedge at the crush front drove the main central delamination crack. The splaying of the lamina bundles observed in the quasi-static crush test and in the dynamic crush test can therefore be categorized into two crush

Table 1 Energy absorption performance (a)

Test Specimen	Impact Velocity/ Constant Velocity (m/s)	Peak Crush Force (kN)	SSCF (kN)	Crush Force Efficiency	Total Crush Distance (mm)	Total Energy Absorbed (kJ)	Total SEA (kJ/kg)
I	0.001	31.86	24.03	1.33	58.48	1.420	87.11
II	2.00	31.01	17.71	1.75	49.29	0.891	67.89
III	5.00	27.88	17.80	1.57	45.67	0.825	67.53
IV	10.00	35.69	18.04	1.98	41.62	0.741	67.04

responses, the global splaying failure and the local fragmentation failure respectively. These identified varied crush response are accredited by the authors to the strain rate dependency of the epoxy resin where an increase in stiffness and a reduction in toughness are introduced at higher loading rates. Referring to the work by Gilat et.al, it was reported that an increase in Young's Modulus (material stiffness) was observed in an epoxy resin with a change of loading condition from quasi-static to dynamic [15]. This was attributed to the extent of which changes in the intramolecular configuration (shape of the polymer chains) can occur in the matrix relative to the time scale of the test. In a dynamic loading condition, due to the short time scale, only intermolecular interactions between polymer chains occur whereas in a quasi-static loading condition, these interactions are extended to the intramolecular level. This promotes a ductile behaviour observed in the quasi-static tests and increases the extent of matrix damage away from the crush front in the form of the central delamination failure crack as observed in the HRCT-scan images comparing the two loading conditions. The length of this central delamination crack controls the radius of curvature of the splaying lamina bundles and therefore the hoop stress in the lamina bundles. This determines the number of axial cracks that create the fronds as seen in the test specimens of the quasi-static crush test and not in the dynamic crush tests which have a more brittle failure.

Increased energy absorption in the quasi-static crush test can be attributed to the differences in the length of the splaying lamina bundles and hence contribution to the overall energy absorption in both the test conditions. The presence of the longer lamina bundles increases the number of energy absorbing mechanisms [14] which include hoop cracking and the frictional resistance between adjacent plies of the lamina bundles upon delamination, and friction at the lamina bundles-loading platen interface.

From increasing impact velocity, a small reduction in the SEA is brought about from the increase in the material stiffness (brittle nature) that reduces the length of the splaying lamina bundles and hence the energy absorbing abilities of the specimen (SEA). However, this change in the material stiffness for loading velocities increasing from 2.0 to 10.0 m/s is relatively small compared with that between the two loading regimes, quasi-static and dynamic.

5 Effect of Stacking Sequence on Identified Response Modes

The phenomenon of the two different response modes (global splaying failure and local fragmentation failure) identified above has been further investigated in the following experimental work on the effect of stacking sequence in the crushing response and energy absorption performances of the carbon-epoxy segment specimens. Test specimens were manufactured from the ACG MTM44-1FR/468 four harness fabric pre-preg material system. This pre-preg material was developed to possess an equivalent performance to the standard

Hexcel M18/1 pre-preg material, and suit out-of-autoclave manufacture that reduces overall costs and time for manufacturing. Test specimens investigated consisted of 2 varied stacking sequences $[(0/90)_2]_s$ and $[(\pm 45)_2]_s$ and tests were carried out both quasi-statically and at an impact velocity of 10.0 m/s, as indicated in Table 2.

5.1 Quasi-static Crush Test

The quasi-static crush test was conducted in accordance to the test procedure previously presented for test specimen (I). From analysing the crushing process of the two quasi-static crush tests conducted, it was observed that the test specimens displayed two different failure modes. The test specimen (V) with a $[(0/90)_2]_s$ stacking sequence exhibited a crushing process consistent with the crushing mode observed in test specimen (I) since both specimens consists of identical stacking sequences. The test specimen (VI) with the $[(\pm 45)_2]_s$ stacking sequence exhibited a different crushing process. Figure 10 presents images taken from the high speed camera of the quasi-static crush test conducted on this specimen. Image (b) illustrates the test specimen responding in a global buckling mode. Figure 10c to e show the test specimen undergoing further buckling, where the left side of the test specimen is bulging out and the right side is caving in. Figure 10f shows the fracturing of the test specimen at a 45.0° angle on its right side where it was collapsing and Fig. 10g presents the test specimen failing in a catastrophic manner.

5.2 Dynamic Crush Test

The dynamic crush test was performed in accordance to the test procedure previously presented for test specimen (IV) at an impact velocity of 10.0 m/s. From analysing the crushing process of the two dynamic crush tests conducted on test specimen (VII) and (VIII), it was observed that the test specimens displayed similar brittle failure modes and crushing process when compared to the test specimen (IV) crush test.

Figure 11 shows the fractured test specimens from this experimental investigation. Specimens (V) and (VI) were tested quasi-statically. The crushed down specimen (V) with the $[(0/90)_2]_s$ stacking sequence is similar to test specimen (I) previously tested with the presence of long inner and six outer fronds. Test specimen (VI) with a $[(\pm 45)_2]_s$ stacking sequence presents a ductile-type failure with partial splaying of the lamina bundles but no well defined splitting into fronds. In the 10.0 m/s tests, specimen (VII) displayed brittle failure similar to (IV), with the same stacking sequence. The lamina bundles of specimen (VIII) with the $[(\pm 45)_2]_s$ ply configuration was seen to be longer axially and displayed greater structural integrity than test specimen (VII) in the dynamic crush tests.

Table 2 Energy absorption performance (b)

Test Specimen	Stacking Sequence	Impact Velocity/ Constant Velocity (m/s)	Total Crush Distance (mm)	Total Energy Absorbed (kJ)	Total SEA (kJ/kg)
V	$[(0/90)_2]_s$	0.001	48.90	1.26	98.46
VI	$[(\pm 45)_2]_s$	0.001	48.48	0.83	67.78
VII	$[(0/90)_2]_s$	10.00	43.14	0.85	75.66
VIII	$[(\pm 45)_2]_s$	10.00	42.94	0.82	76.96

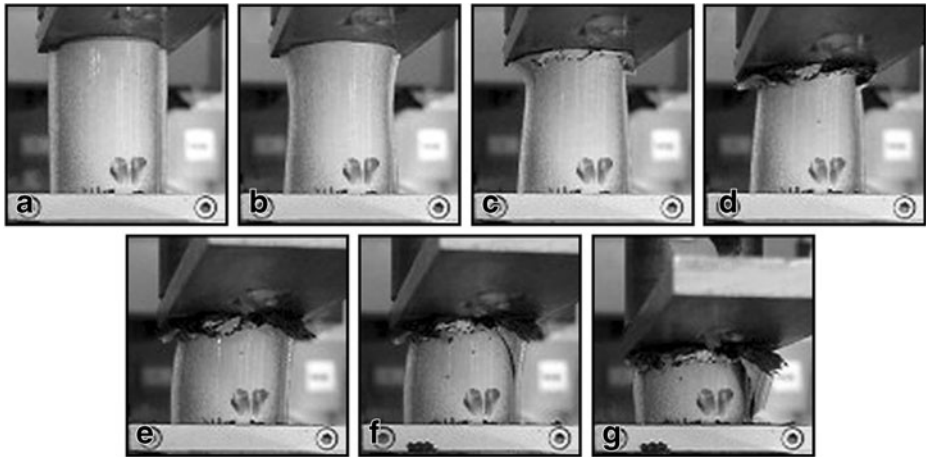


Fig. 10 Quasi-static crushing process in specimen (VI) with a stacking sequence of $[(\pm 45)_2]_s$

6 Results and Discussion (b)

The plot of the crush load–displacement (see Fig. 12) from the crush tests of test specimens (V), (VII) and (VIII) is similar to that of a typical progressive crush load–displacement curve for a composite tube. It consists of four main phases namely, initial crush load increase to a peak value, rapid crush load drop, crush load saturation and lastly steady state crushing. The test specimen (VI) on the other hand displays different behaviour to those mentioned above. After the trigger phase no progressive crushing was established as the specimen collapsed in

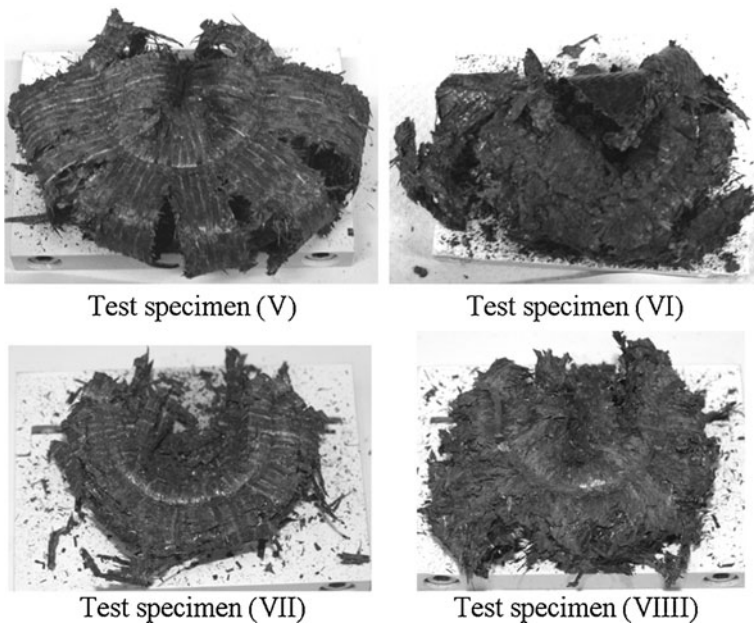


Fig. 11 Test specimens crushed in quasi-static and dynamic crush tests

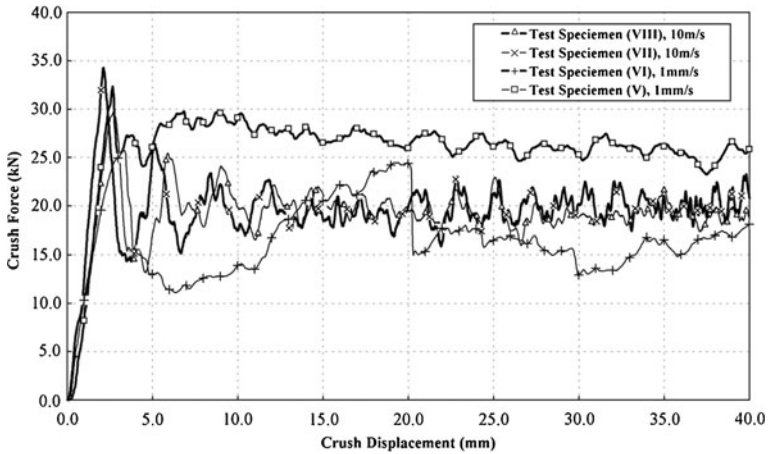


Fig. 12 Crush force versus Crush Displacement (b)

a global buckling mode, characterised by large amplitude oscillations in the crush force levels, until a sudden significant drop after approximately 20.0 mm, as the test specimen fractured (see Fig. 10c) and failed catastrophically.

Table 2 summarizes the energy absorption performances of the test specimens for the entire duration of the crushing process. The highest SEA was achieved by the test specimen with a $[(0/90)_2]_s$ stacking sequence in the quasi-static crush test. A 30.0 % reduction in the SEA in the dynamic crush test was calculated when comparing between the test specimens of the $[(0/90)_2]_s$ stacking sequence. The lowest SEA was reached by the test specimen with a $[(\pm 45)_2]_s$ stacking sequence in a quasi-static loading condition that proceeded into a global buckling mode before failing catastrophically. In the dynamic crush test, the test specimen with a $[(\pm 45)_2]_s$ stacking sequence attained a SEA value of 1.72 % higher than the test specimen with the $[(0/90)_2]_s$ stacking sequence. In this case both specimens failed at the crush front in a brittle fracture mode, which may explain why the stacking sequence had no significant influence on SEA.

6.1 Response Mode

The identified phenomenon presented in this paper of the two different response modes (global splaying failure and local fragmentation failure) is observed in greater detail from the quasi-static and dynamic loading of the test specimen with a $[(\pm 45)_2]_s$ stacking sequence. Global buckling followed by the catastrophic failure of the test specimen in the quasi-static crush test was due to a considerably reduced axial stiffness from the absence of axial 0° fibres when compared to the axial stiffness of the $[(0/90)_2]_s$ test. This effect was not seen in the dynamic crush tests of the $[(\pm 45)_2]_s$ test specimen because of the local fragmentation failure mode. Therefore, in the quasi-static crush test the whole test specimen was loaded (refer to Fig. 10b, where the specimen is seen to bulge and cave in) and eventually succumbs to global buckling. In the dynamic crush test however, the $[(\pm 45)_2]_s$ test specimen was loaded locally (close to the crush front) and in combination with the increased stiffness of the matrix, progressive crushing was thus achieved.

For the $[(0/90)_2]_s$ test specimen, the fracturing of the lamina bundles can be seen to occur predominantly in the longitudinal direction of the test specimen (see Fig. 11). This is unlike

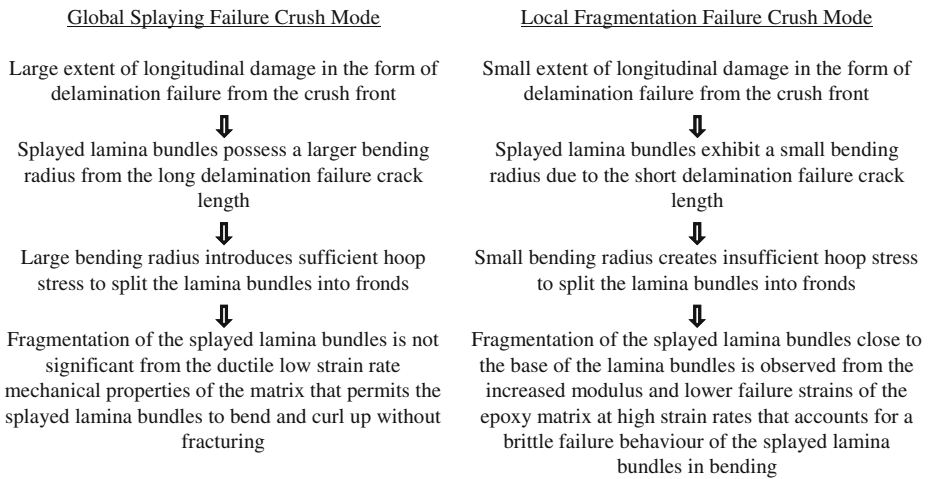


Fig. 13 Flowchart of crushing response processes

the $[(\pm 45)_2]_s$ test specimen where failure strains in the segment axial and hoop directions of the $\pm 45^\circ$ plies is very high ($>10.0\%$ strain recorded from material coupon test data) so that in quasi-static tests there is no hoop splitting and in the 10.0 m/s test the lamina bundles were observed to exhibit fracture further away from the base of the lamina bundles (see Fig. 11). It should also be noted that for the fabric composite plies rate effects are highest for loads applied at $\pm 45^\circ$ to the fibres where behaviour is matrix controlled, which explains why the $[(\pm 45)_2]_s$ segments have the most significant change in failure mode between quasi-static and dynamic tests from global buckling at low rates to brittle fracture at high rates. It is interesting to note that the difference in the laminate sequence is less significant in improving the energy absorption when progressive crushing takes place (at 10.0 m/s) an improvement in the structural integrity of the crushed specimen is attained in the $[(\pm 45)_2]_s$ segments due to the longer lamina bundles.

7 Conclusion

In this investigation of chamfered tube segment specimens, a successful methodology for both the testing and the analysis has been implemented to study and compare the crushing characteristics and the energy absorption performances in both quasi-static and dynamic loading conditions. The testing methodology included the use of a high speed camera to capture the crushing behaviour of the test specimens during the crush tests. In addition to capturing the crushing behaviour of the test specimens during the crush tests, High-resolution Computed Tomography (HRCT) scanning of the test specimens was performed to enable a detailed analysis of crushed test specimens. The analysis methodology used the measured load–displacement data from the test machine to calculate the energy absorption performances in terms of Crush force efficiency (CE), Energy Absorbed (EA) and Specific Energy Absorbed (SEA). Most tests were carried out on segments with $[(0/90)_2/0/(90/0)_2]$ ply layouts. The test specimen in the quasi-static crush test exhibited the highest energy absorption performances when compared to the test specimens in the dynamic crush tests. There was not a significant difference in EA in the 3 dynamic tests in the range 2–10 m/s; however all the dynamic tests showed significantly less EA than the quasi-static test. This is

an important effect which should be taken into account in the design of composite energy absorbing systems.

This difference in crushing behaviour which was identified from the work presented is attributed to varied crushing modes and the varied characteristics of the lamina bundles due to the strain rate dependent epoxy matrix. A flowchart representing the crushing response processes in these two modes is presented in Fig. 13. Depending on the response mode, this determined the crushing behaviour of the test specimens. The crushing behaviour of the test specimens in the quasi-static and dynamic crush tests were essentially in the splaying mode, with the lamina bundles in the dynamic crush tests closer to the brittle fracturing crushing mode. When comparing the energy absorption performances of the test specimens in the dynamic crush tests, it was found that the energy absorption performances do not vary much due to the extent of changes in the material properties at the dynamic strain rate regime. Additional quasi-static and dynamic crush tests on segments with an alternative stacking sequence $[(\pm 45)_2]_s$ with mainly $\pm 45^\circ$ plies supported the influence of strain rate on failure mode. In $\pm 45^\circ$ composite specimens strain rate effects are more significant due to the properties being matrix dominated. Here it was found that in the 10.0 m/s tests at higher rates crush failures were due to brittle fracture at the crush front, with SEA values close to the $0^\circ/90^\circ$ specimens. However the quasi-static failure behaviour was dominated by global buckling due to the low axial stiffness at low rates in the segment walls, with no steady crushing and lower SEA. For the design of absorber elements, this emphasises the importance of designs and fibre layups which avoid global buckling and fail by local crush front fracture. In the case of dynamic loads, failure is more likely to be localised since crush failure is initiated before there is time for global buckling to take place. When this occurs the ply stacking sequence does not appear to be critical for energy absorption, and the addition of $\pm 45^\circ$ plies can enhance structural integrity.

Acknowledgments The author would like to thank Cooperative Research Centre for Advanced Composite Structures (CRC-ACS), Melbourne for providing the test specimens and clamps under a collaboration project between DLR and CRC-ACS. The author also extends his sincere gratitude to his DLR colleagues Husam Abu El-Hija, Harald Kraft and Raouf Jenmali for their assistance and guidance in conducting the crush tests and HRCT scans.

References

1. Feraboli, P., Wade, B., Deleo, F., Rassaian, M.: Crush energy absorption of composite channel section specimens. *Compos. Part A: Appl. Sci. Manuf.* **40**(8), 1248–1256 (2009)
2. Kindervater, C., Thomson, R., Johnson, A., David, M., Joosten, M., Mikulik, Z., Mulcahy, L., Veldman, S., Gunnion, A., Jackson, A., Dutton, S.: Validation of crashworthiness simulation and design methods by testing of a scaled composite helicopter frame section. In: *American Helicopter Society 67th Annual Forum*. American Helicopter Society International, Inc (2011)
3. Johnson, A., David, M.: Failure mechanisms in energy-absorbing composite structures. *Philos. Mag.* **90** (31), 4245–4261 (2010)
4. Jackson, A., David, M., Gunnion, A., Kelly, D., Dutton, S.: Dynamic and quasi-static crush testing of closed carbon-fibre/epoxy elements. In: *27th Congress of International Council of the Aeronautical Sciences*. International Council of the Aeronautical Sciences (2010)
5. Kirsch, P., Jannie, H.: Energy absorption of glass polyester structures. *SAE Technical Paper Series* (810233) (1981)
6. Mamalis, A., Manolacos, D., Demosthenous, G., Ioannidis, M.: The static and dynamic axial crumbling of thin-walled fibreglass composite square tubes. *Compos. Part B: Eng.* **28**(4), 439–451 (1997)
7. Thomson, P.: The crush behavior of pultruded tubes at high strain rates. *J. Compos. Mater.* **24**(6), 594–615 (1990)
8. Schmueser, D.W., Wickliffe, L.E.: Impact energy absorption of continuous fiber composite tubes. *J. Eng. Mater. Technol.* **109**(1), 72–77 (1987)

9. Kindervater, C.: Energy absorption of composites as an aspect of aircraft structural crash resistance. In: Fourth European Conference on Composite Materials. pp. 643–651 (1990)
10. Farley, G.: The effects of crushing speed on the Energy-Absorption capability of composite tubes. *J. Compos. Mater.* **25**(10), 1314–1329 (1991)
11. Mamalis, A., Robinson, M., Manolacos, D., Demosthenous, G., Ioannidis, M.: Crashworthy capability of composite material structures. *Compos. Struct.* **37**(2), 109–134 (1997)
12. Jacob, G., Fellers, J., Simunovic, S., Starbuck, J.: Energy absorption in polymer composites for automotive crashworthiness. *J. Compos. Mater.* **36**(7), 813–850 (2002)
13. Schultz, M., Hyer, M.: Static energy absorption capacity of Graphite-Epoxy tubes. *J. Compos. Mater.* **35**(19), 1747–1761 (2001)
14. Hull, D.: A unified approach to progressive crushing of fibre-reinforced composite tubes. *Compos. Sci. Technol.* **40**(4), 377–421 (1991)
15. Gilat, A., Goldberg, R., Roberts, G.: High strain rate response of epoxy in tensile and shear loading. *J. Phys. IV (Proceedings)* **110**, 123–127 (2003)